

# Low frequency recovery for ambient seismic data from ultra-dense linear arrays

Iga Pawelec\* & Paul Sava\*

\* Center for Wave Phenomena and Dept. of Geophysics, Colorado School of Mines, Golden CO 80401  
email ipawelec@mines.edu

## ABSTRACT

Although with the advent of wireless nodes seismic data are commonly acquired as continuous-time recordings, most of the information not related to active source efforts is discarded. Ambient data are a valuable source of low frequency information, with the potential to enhance near-surface characterization using surface waves. We demonstrate that geophone correction plays an instrumental role in recovering low frequency signals from geophone arrays is possible down to as low as 1% of geophone's natural frequency. Using the continuous seismic data recorded on an ultra-dense linear array of 10 Hz geophones, we show that ambient data correlations in 0.1-1 Hz band are primarily sensitive to local traffic moveouts, and thus limiting their utility to deriving information about attenuation. However, the recorded coherent signals at these frequencies are potentially valuable for velocity inversions when recorded on a large enough 2D array. The correlations obtained from inline traffic data in 2-20 Hz band show moveouts corresponding to local surface wave velocities and thus can be used for near surface shear wave velocity inversions. Comparing the phase velocity spectra generated from an active shot with that computed from a virtual gather reveals good agreement in the 5-15 Hz band, proving the validity of interferometric gathers as the source of information about shear wave velocities, even in areas with no active source data.

**Key words:** low frequency, passive seismic, interferometry

## 1 INTRODUCTION

In land seismic acquisition, receivers are much smaller and easier to deploy than sources. Although efforts are made to create low-impact portable land sources (Châtenay, 2019), the real land acquisition revolution over the last two decades focused on receivers. Since early land wireless systems (Wilcox, 2015), land nodes have evolved, shrinking in size, providing longer battery life and reducing the seismic signal distortion (Dean et al., 2018). The shift from cabled to wireless acquisition is primarily motivated by the need for higher productivity and trace density in exploration seismology (Mougenot, 2004; Freed, 2008; Manning et al., 2018), however 3C land nodes are also an increasingly popular choice for short-time deployments in observational seismology (Ward and Lin, 2017; Wang et al., 2017). Two important consequences of introducing autonomous nodes are the geometry design flexibility, and the ability to select the record length after rather than before data acquisition.

Analyzing continuous data before and after triggering active source can provide valuable information about noise affecting active data quality (Pawelec and Sava, 2020). But can it tell us more than that? Can we use the entire volume of continuous data, including quiet times without active sources, to improve the processing and interpretation of active source data? To answer these questions, we investigate data acquired during the 2017 CSM geophysical field camp with an ultra-dense linear geophone array formed with 392 10 Hz nodes provided by GTI. The main focus of our investigation is on characterizing signals recorded in the ultra-low (0.1-1 Hz) and low (2-20 Hz) frequency bands and assessing their utility for deriving near-surface shear wave velocity profiles.

We show that despite the inherently low sensitivity to low frequencies, geophones are capable of recording coherent and meaningful signals at frequencies as low as 1% of their natural frequency. We present several examples of such signals, including

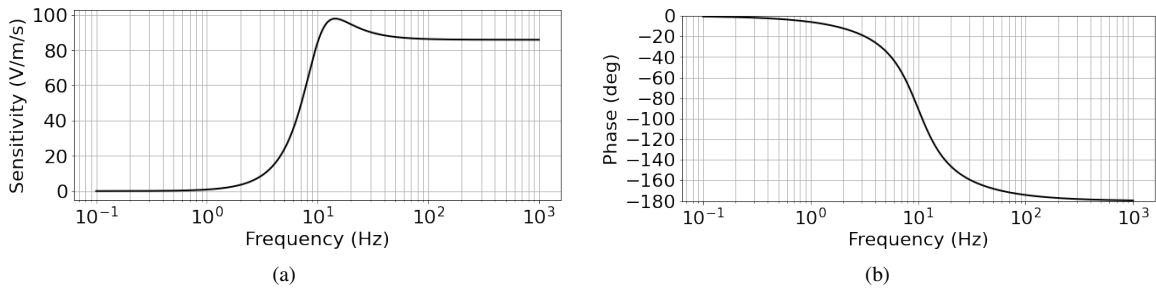


**Figure 1.** (a) Amplitude and (b) phase response of a geophone with  $G_0 = 85.8$  V/m/s,  $\omega_0 = 20\pi$  rad/s and  $\lambda = 0.51$ .

ringing events with infinite apparent velocity, signals corresponding to the motion of vehicles present on the acquisition site, and mysterious coherent events propagating with slow velocities that might be weather-related. Through the interferometric processing we find that virtual shots generated from 0.1-1 Hz ambient data primarily indicate the velocities of local traffic while the 2-20 Hz data also sensitive to the local shear wave velocities. Given the difficulty of generating signals below 1 Hz with active sources, ambient data have the potential to enhance the low frequency resolution of phase velocity spectra obtained from active data, thus increasing the depth of investigation and improving the near surface model for statics computation.

## 2 GEOPHONE SIGNALS AT LOW FREQUENCIES

### 2.1 Geophone impulse response

Geophones use a coil around a magnet which, according to Faraday’s Law of magnetic induction, responds to the velocity of the proof mass (Hons and Stewart, 2006). When the measured frequencies match the natural frequency of the geophone, its output is nearly proportional to the ground particle velocity (Hons and Stewart, 2006). The ratio of geophone output voltage to the input ground motion is described by the geophone equation,

$$H(\omega) = G_0 \frac{\omega^2}{-\omega^2 + 2i\lambda\omega_0\omega + \omega_0^2}, \quad (1)$$

where  $G_0$  is the geophone sensitivity expressed in V/m/s,  $\omega_0$  is the natural angular frequency, and  $\lambda$  is a dimensionless damping ratio. Equation 1 implies that amplitudes roll off below  $\omega_0$  and a phase shift is introduced around geophone’s natural frequency. Figure 1 illustrates an example geophone response for a high-sensitivity 10 Hz geophone with  $\lambda = 0.51$ . Note that the most significant phase shift occurs between 1 and 100 Hz while the peak sensitivity is at about 14 Hz and stabilizes between 60 Hz and the Nyquist frequency. Below 14 Hz, the sensitivity is approximately proportional to the frequency squared which has important implications for recovering low frequency content from geophone data, as discussed later.

Monk (2020) demonstrates the negative consequences of neglecting the instrument response correction on the coherence of low frequency data after spiking deconvolution. Since SNR at the low frequency end of the spectrum is often quite low, the noisy components can dominate phase estimation at such frequencies. Applying instrument response correction (e.g., by spectral division using equation 1) brings low frequencies closer to the level of high frequencies, thus limiting their impact on phase estimations and ensuring better phase coherence after deconvolution.

Ambient data can have similarly small SNR at low frequencies, especially in the presence of strong near-surface heterogeneity. Thus, if the bandwidth of interest includes frequencies below the geophone natural frequency, the instrument response correction should be applied to reduce the effect of phase shift and amplitude distortion in the subsequent interferometric processing. Figure 2(a) shows the power spectrum computed from raw data spanning 5 days, averaged with 20 bins per octave. The expected drop in power below 10 Hz can be observed for most receivers, but some maintain strong signal down to DC component. This behavior is due to instrument clipping triggered by heavy vehicles or Vibroseis shaking next to a node. If such signal reaches amplitudes close to the geophone’s maximum signal level, the entire derived spectrum is affected, and information from quiet times of low signal levels is not represented accurately. Muting portions of the affected traces is needed to avoid boosting outliers in the corrected traces. Furthermore, the correction needs to be limited to the frequency band not affected by instrument thermal DC component for stability, as discussed next.

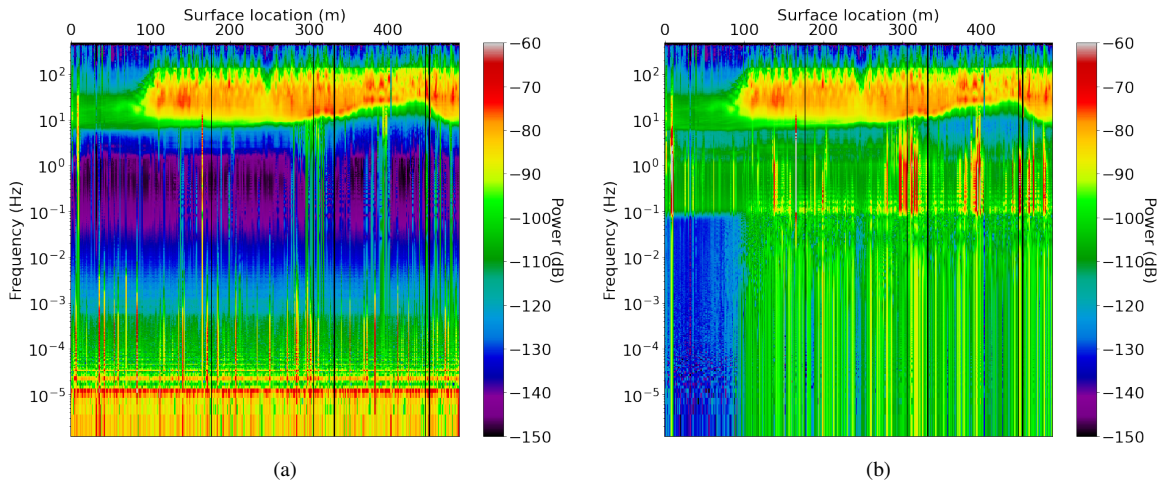


**Figure 2.** Power spectrum as a function of surface location before (a) and after (b) the geophone correction and 0.1 Hz lowcut filter. Note the significant drop in frequencies below 10 Hz except for several nodes that have anomalous behavior and appear to have strong energy almost to DC component.

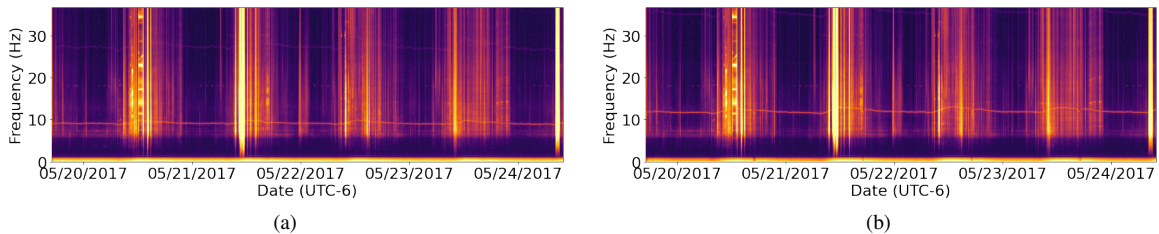


**Figure 3.** Spectrograms for two adjacent geophones separated by 1.25 m computed from raw data. Note the near-DC thermal trend and the diurnal trends centered at 10 and 12 Hz, respectively.

## 2.2 Geophone thermal response

To get meaningful ambient data correlations, we need to ensure that the recorded signal is related to ambient sources and not to the instruments themselves. For DAS measurements, this consideration is not as prevalent since the measuring device is a continuous cable and thus the noise is not truly location-independent. Conversely, with blind nodes each sampling location provides an independent measuring point. This is a challenge since each node can be exposed to different soil conditions, ground coupling, and tilt. A power spectrum computed for each sampling location, such as the one shown in Figure 2, gives a quick way of looking at data over multiple bands of interest. If equation 1 was valid across the entire bandwidth, the most likely explanation for the observed high amplitudes below 0.1 Hz would be that seismic signals in that bandwidth are orders of magnitude stronger than the higher frequency signals. However, the geophone equation is limited to describing instrument behavior for  $\omega \approx \omega_0$  and thus is unlikely to be accurate for frequencies as low as  $10^{-5}$  Hz. If we examine the time-frequency distribution of these low-frequency trends (Figure 3), we can notice that their intensity changes over the course of a day. This is because the instrument response changes as a function of temperature, with the “thermal DC” being a first order effect that is usually mitigated by a low-cut filter or a detrending procedure. One might be interested whether only the low frequencies are affected by temperature changes. The short answer is no. Note the strong diurnal trend centered at different frequencies (10 Hz and 12 Hz, respectively) in Figure 3. The spectrograms come from the two adjacent nodes separated by 1.25 m, so these signals are unlikely to be a subsurface response. Similar observations were made for 3C Fairfield Nodal Zland nodes in different acquisition settings: Johnson et al. (2019) report that ambient data are impacted by instrument noise modulated by temperature and wind conditions and related to the instrument coupling. Farrell et al. (2018) observe that an 11 kg weight on top of a node impacts the instrument noise band. We conclude that temperature is also one of the main driving factors of the instrument self-noise observed during the CSM field camp. In the following section, we show that with careful processing accounting both for geophone impulse response and its low frequency thermal response we can recover high quality geophone data at frequencies as low as 0.1 Hz.

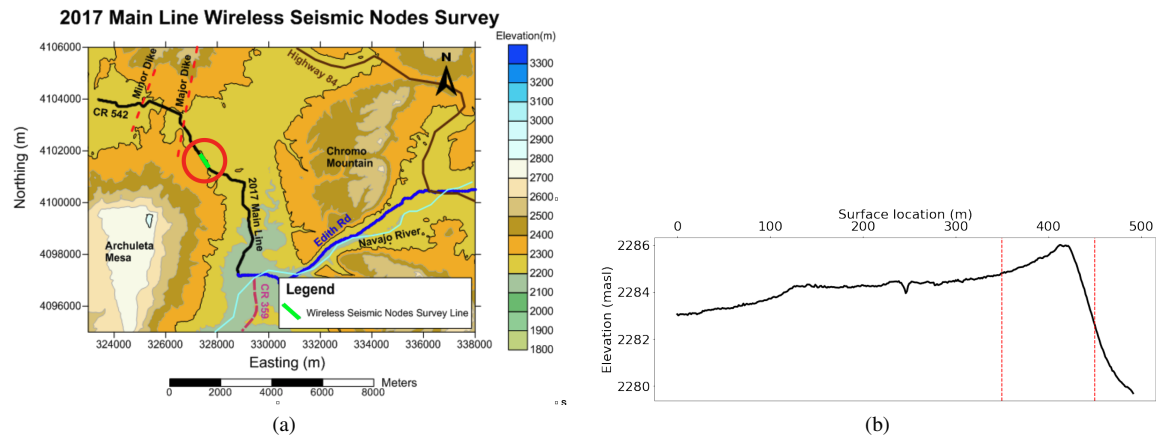


**Figure 4.** (a) Approximate location of the nodal survey and (b) elevation profile along nodal line. Note that the maximum absolute elevation change is less than 6 m.

### 3 SURVEY LOCATION AND PARAMETERS

The studied dataset was acquired as a part of the Colorado School of Mines geophysical field camp. The acquisition site south of Pagosa Springs (south-west Colorado) is illustrated in Figure 4(a). This area is known for its geothermal system, including the world’s deepest hot spring (Mochan, 2011). A linear array of GTI 392 blind nodes was deployed for 5 days, with a receiver spacing of 1.25 m with the objective of comparing nodal and cabled geophone arrays and evaluating the benefits of super fine sampling. Recording time included active seismic sources with Vibroseis non-linear upsweep between 4-140 Hz with 10 m shot spacing, as well as the quiet night-time at a sparsely populated area (Figure 4(a)). Multiple shot points were skipped on the north-west side of the array, including all shots between 0-100 m. The skipped shots are the reason for the 0-100 m weak signal area in Figure 2(a).

The objective of our continuous data analysis is to establish the lowest usable frequencies present in ambient geophone data, characterize signals at low frequencies, and evaluate their potential for enhancing the processing and interpretation of active source data. At the lowest end of the spectrum in Figure 2(a), the high signal amplitudes are caused by geophone’s thermal response. Extracting the relevant seismic signals from data below 0.1 Hz might be possible with advanced processing, but in this report we focus our attention on the ultra-low band between 0.1-1 Hz and 2-20 Hz band. We show that with the minimal amount of processing aimed at restoring the true amplitude ratios geophone data can provide valuable information about the ambient noise background at frequencies as low as 1% of geophone’s natural frequency. For both analyzed bands, we select data windows corresponding to inline traffic and form virtual shot gathers to assess data utility for deriving shear wave velocity profiles based on phase velocity spectra. While the only geologically-relevant information that can be derived from the ultra-low bandwidth pertains to the identified region of strong signal attenuation, traffic data between 2-20 Hz are sensitive to the local shear wave velocities and can be used to augment active data information, especially in the area where source points were skipped. The following sections provide details on data processing, the signals found in the ultra-low frequency band, and the interferometric results for both analyzed bands.

## 4 AMBIENT NOISE ANALYSIS

### 4.1 Processing

For the purposes of our analysis, we limit data processing to geophone correction, thermal DC suppression and bandpass filtering. Since Figure 2(a) reveals outlier low frequency response at several locations, we do not recommend applying geophone correction to the instruments with abnormal spectra. Figure 5 shows an example spectra for a geophone correction implemented down to 1 Hz for two 5-days long traces. As expected from examining amplitude and phase response from Figure 1, the geophone correction boosts low frequencies (Figure 5(a)) below 10 Hz. An additional step can be taken to suppress instrument’s thermal response, either by applying a detrending procedure or a lowcut filter. However, applying the correction to a trace whose spectrum is anomalous leads to the undesired behavior (Figure 5(b)), compromising data quality for such a trace. In Figure 2(b), the effect of correction on such faulty traces is even clearer. We determine that the leading cause of the unusual raw data spectra are the high energy events that result in instrument clipping. Since the spike-like behavior in time domain spreads through the entire frequency domain, the

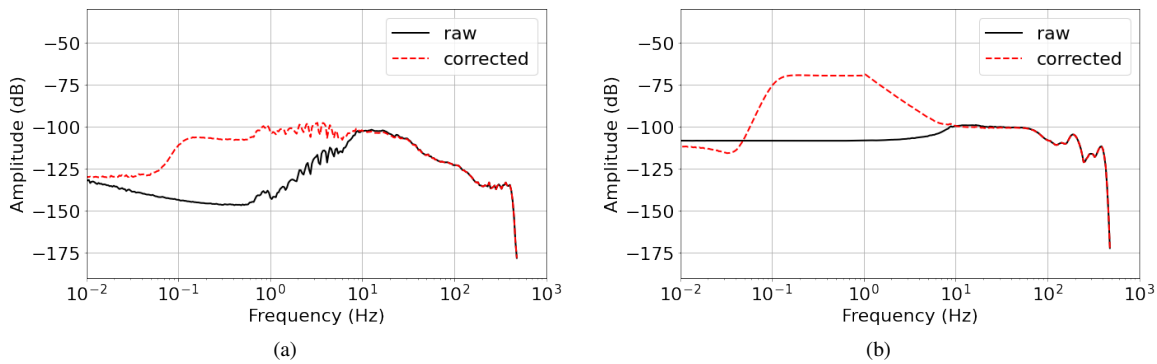


**Figure 5.** Geophone correction applied down to 1 Hz for (a) a typical trace and (b) trace with abnormal low frequency behavior. The spectrum in (b) is a result of instrument clipping, during strong energy events.

resulting data spectrum is not a reliable representation of data at the affected sampling location. To address this problem, we zero out the affected data and interpolate the values from the adjacent traces. Alternatively if subsequent analysis is intended on the windowed data, each window would need to be individually. In the latter case, the windows containing clipping events can be rejected from further analysis using a simple RMS-based criterion.

#### 4.2 Seismic signals in the ultra-low bandwidth

Due to geophones' insensitivity at low frequencies, data at frequencies significantly lower than the geophones natural frequency are rarely analyzed, and when they are, they tend to be of poor quality. In Figures 6 - 8, we present examples of signals recorded by the dense linear geophone array at frequencies between 0.1 and 1 Hz, that is 100-10 times less than geophones' natural frequency of 10 Hz. To emphasize the role of geophone correction on data quality in that bandwidth, we present the same signals without and with correction. We divide the identified full-array coherent signals into three main classes: persistent ringing events of infinite apparent velocity, coherent slow-moveout events with no evident source, and events associated with inline traffic. We discuss each class in the following paragraphs.

Figure 6 shows a 200 s long window with the ringing infinite velocity event. Although 200 s of the data are shown, the signal can be observed for about 20 min, with several occurrences of similarly looking signal throughout the 5 recording days. The origin of the signal is unknown and the directional information cannot be derived from the linear array, but given the bandwidth under consideration and infinite apparent velocity, the source is likely to be a significant distance away in the crossline direction. Comparing the bandpassed data to data with geophone correction and bandpass reveals several notable differences. First, the background noise character is different on both panels. Data without the geophone correction has noise background that appears as incoherent high-frequency noise, with a localized moving disturbance standing out between 340-490 m. That disturbance appears to vanish in the geophone corrected data and the background noise becomes more coherent and lower frequency. The signal itself is interpretable on both panels, with early times between 20-50 s looking more coherent in Figure 6(a) and later times (150-200 s) easier to pick in Figure 6(b). The explanation for this phenomenon is the relative strength of signal to the background noise at each frequency within the data bandwidth. After geophone correction, data at each corrected frequency should be represented at their true relative strength. That is the case to the extent, however the manufacturing uncertainty in the geophone parameters and the frequency assumption behind the geophone equation causes the amplitudes to be approximately at their relative strength, provided that no time domain spikes distort data spectra prior to correction. As a result, the natural microseismic noise becomes much louder, but so does the coherent signal. Therefore, the SNR as a function of frequency is different for the two data panels, with high frequency noise dominating in Figure 6(a) and low frequency noise more prominent in Figure 6(b).

The second type of signal we identified is exemplified by Figure 7. Since this signal is relatively weak, in addition to showing the effect of instrument correction, we also show data after wavelet denoising. The panels show a sequence of slow events that look mostly linear at early times but show curvature at later times. The origin of this signal is unknown but the observed moveouts suggest that the source is on the north-west side of the array and, given slow propagation velocities, might be wind-related. Similarly to the previous example, geophone correction shifts the frequency-dependent SNR. However, the signal clarity improvement is more apparent in this case due to carrier frequency being lower than in Figure 6. Note in particular the sequence of arrivals between

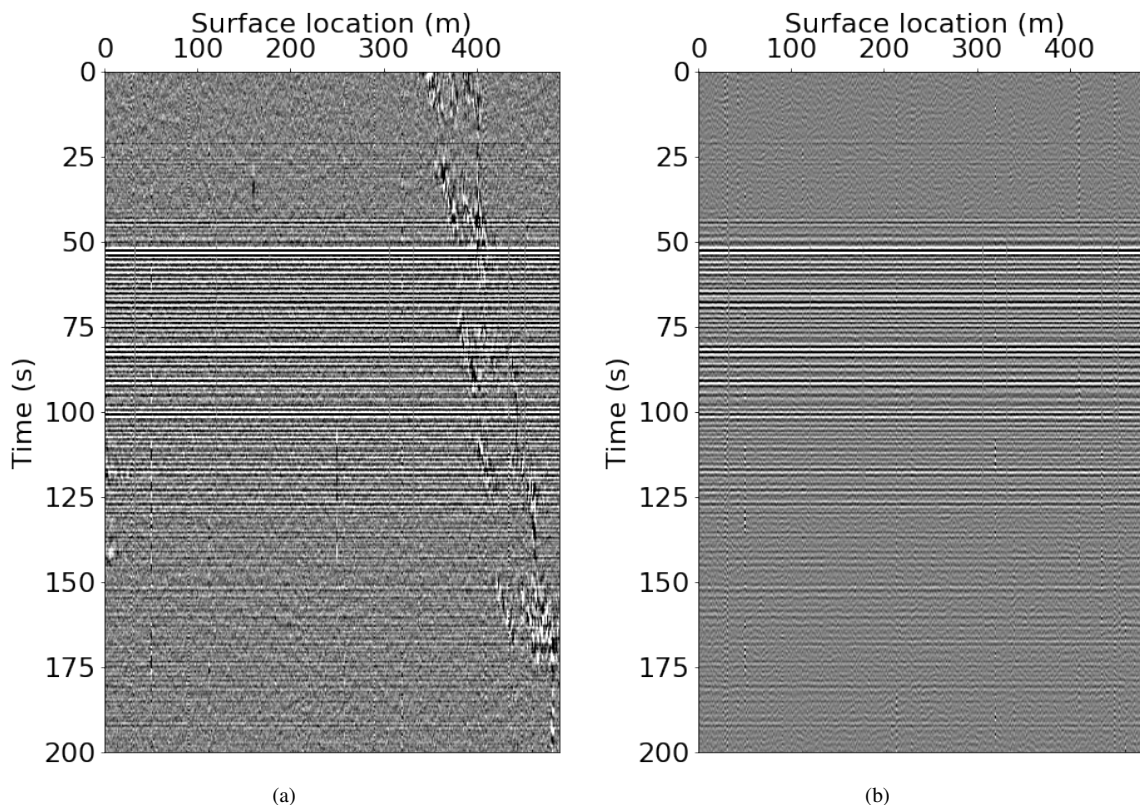


**Figure 6.** Ringing coherent noise of infinite apparent velocity recorded on a linear geophone array. Panel (a) shows raw data after 0.1-1 Hz bandpass filter while panel (b) shows data after geophone correction applied down to 0.1 Hz followed by 0.4-1 Hz bandpass filter. Note the difference in the background noise and SNR for the two panels.

100-125 s that is easily tracked for geophone corrected data and challenging to pick on data without correction, even when denoising procedure is applied.

The third and final signal type we discuss is traffic data shown in Figure 8. In the ultra-low frequency band, the geophones pick up vehicle motion along the array, with moveout corresponding to vehicle speed as a function of time. The difference between raw bandpassed data and geophone corrected data is drastic, with the strong trail of incoherent noise following the moving vehicle in the raw data and disappearing in corrected data. Similarly to the previous examples, this can be attributed to shifting the frequency-dependent SNR and correcting for small phase shifts between 0.1-1 Hz (recall the difference in phase response depicted in Figure 1(b)). That observation has practical consequences for interferometric data processing: as we show next, implementing geophone correction before correlation improves the continuity and phase fidelity in the derived virtual shot gathers.

### 4.3 Interferometric results

We present the results of interferometric processing for 0.1-1 Hz and 2-20 Hz frequency bands and compare the latter to active shot data. Figure 9 shows the correlation panels for the ultra-low frequency band. Panels (a) and (b) are computed from “random noise” data windows while panels (c) and (d) use inline traffic data windows. The observed differences in signal and noise quality between the same data panels result from pre-processing without (panels (a) and (c)) or with (panels (b) and (d)) the geophone correction. The correlations from “random noise” have the majority of coherent energy at positive lags, especially in Figure 9(b). The energy leakage at negative lags in Figure 9(a) can be caused by phase misalignment and amplitude imbalance from not implementing the geophone correction. The energy concentration at positive lags suggests that the majority of the seismic energy comes from the west side of the array, with the moveouts indicating car and train traffic as likely sources. Although the signals after geophone correction are more concentrated and coherent, especially for the slowest event, the corrected panel has notably higher low frequency noise background. This is a direct consequence of correcting the amplitude imbalance. Before geophone correction, signals at 1 Hz are

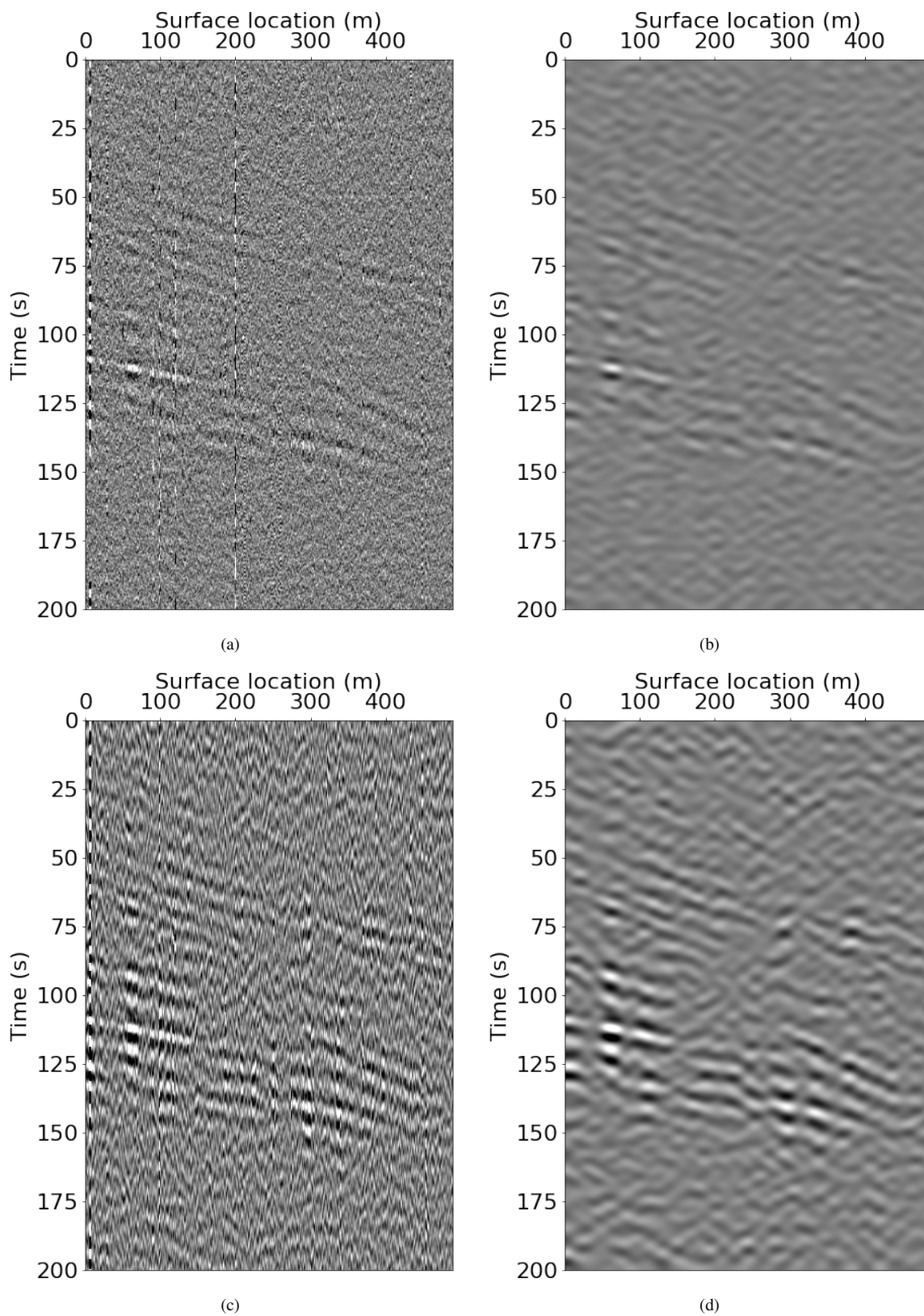


**Figure 7.** Coherent low frequency signal recorded on our dense linear array. Panels (a) and (b) show raw bandpassed data before and after denoising, respectively, while (c) and (d) show data after geophone correction without and with denoising. Note that geophone correction lowered the signal dominant frequency and changed the background noise character.

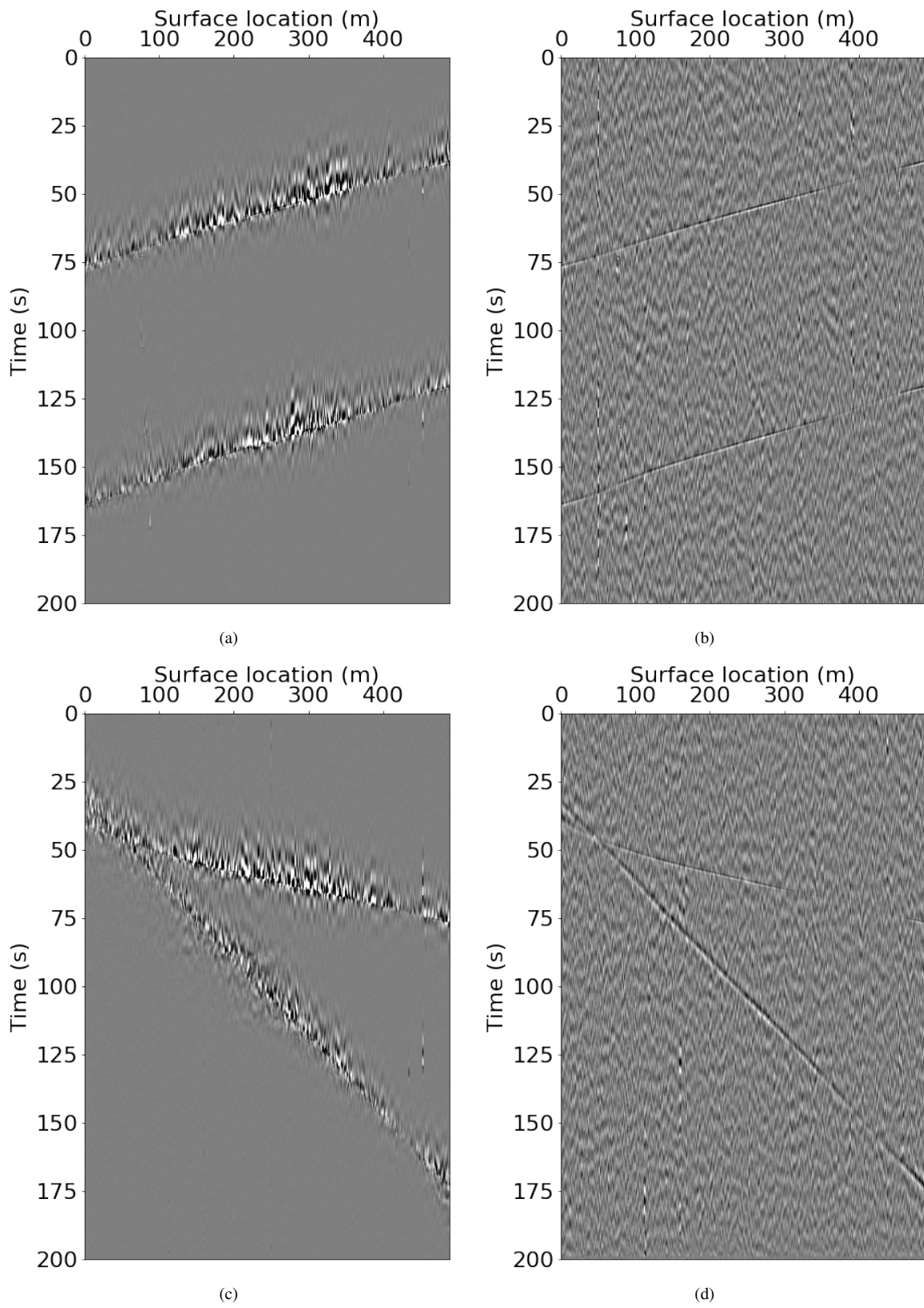


**Figure 8.** Traffic noise in 0.1-1 Hz band. (a) and (c) show raw data after bandpass filter while (b) and (d) show the same data corrected for geophone response before bandpassing. Note that geophone correction improves traffic signal continuity, but also boosts the low frequency noise background.

about 100 times stronger than these at 0.1 Hz. Restoring their natural balance emphasises the true relative strength of coherent energy to the background noise.

The inline traffic correlations show coherent signals for both positive and negative lags, as one could expect from a roadside array registering vibrations from vehicles moving in both directions along the array. The signal continuity is considerably better for the data after geophone correction (Figure 9(d)). In this case the low frequency noise background is not as overwhelming as for the random noise correlations because sources (vehicles) are moving right next to the geophone array and thus the signal generated by them is stronger than the background noise. Another feature of note, that was indicated but not as apparent in the random noise correlations, is the region of strong attenuation at 350-450 m. This region is indicated on the elevation profile in Figure 4(b). The low frequency attenuation effect can also be observed on the power spectra corresponding to the affected locations in Figure 2(a). The combined observations suggest that the attenuation effect is likely caused by a shallow geologic feature which also affects the topographic profile in that area.

Beyond providing insights into frequency-dependent signal attenuation, the utility of ambient data in 0.1-1 Hz band for deriving subsurface information is limited since the observed moveouts correspond to the speed of moving vehicles rather than propagation velocities of surface waves. However, the same is not true about data in the 2-20 Hz band. In general, ambient data from random noise windows could provide valuable low frequency information missing from active source data, but as we discuss in the submitted SEG abstract, linear arrays do not allow for determining the primary direction of the incoming energy, thus leading to phase velocity spectra sensitive to apparent rather than inline velocities. One way to overcome this challenge without repeating the field experiment in a different configuration is to only use data from in-line sources such as cars. In Figure 10 we show an example normalized virtual shot gather created using such data. We combine data from positive and negative lags to improve SNR and compare the virtual gather to the bandpassed active shot acquired at the same location. Note that the surface wave moveouts agree on both panels, but virtual shot data quality drops significantly beyond 300 m. Another interesting example of a virtual gather is shown in Figure 11(b). The dominant energy at 0-200 m corresponds to the surface waves. The gather also shows ample evidence of near surface scattering (multiple diffractions). Similarly to Figure 10(b), the signal character changes drastically around 300 m and continues through the area of strong attenuation at 350-450 m: the signal there is only visible due to normalizing each individual trace. Despite the much narrower bandwidth and lower SNR than that of active data in Figure 11(a), the virtual shot gather provides valuable information about surface wave velocities, as revealed by comparing velocity phase spectra for active data and virtual gather depicted in Figures 11(c) and 11(d). Both spectra look comparable at 5-15 Hz. Furthermore, the virtual shot gather can provide velocity information in places where no active data are available (recall that all shot points between 0 and 100 m were skipped due to nearby infrastructure). Thus, ambient data add value to active recordings.

## 5 DISCUSSION

The ability of conventional geophones to record high-fidelity signals significantly below their natural frequency exceeded our expectations. Unfortunately, the limited aperture of our array and its 1D layout limit the interpretability of some of the discovered low frequency signals. The wavelengths associated with 0.1-1 Hz bandwidth are on the order of kilometers (for example, assuming the dominant velocity of 2000 m/s and frequency of 0.5 Hz, the wavelength would be 4 km). Thus, for a source located far enough from the array, observing the infinite apparent velocity is not surprising. Having a 2D geophone array with a larger spatial extent, as is the case for 3D seismic surveys, would allow for determining the source back-azimuth, and provide precious low frequency velocity information.

Random noise correlations can also give valuable insights about subsurface and local noise sources. However, similarly to strong coherent signals from unknown sources away from the array, the virtual shot gathers created through interferometric processing cannot provide accurate information about velocity structure without knowing the dominant direction of the incoming energy. The asymmetry in positive and negative lags in Figure 9(b) points to the strongest ambient sources being located north-west of the array, providing further motivation for a 2D array deployment to maximize ambient data benefits.

## 6 CONCLUSIONS

Our analysis shows that properly applied geophone correction improves phase alignment and data quality for frequencies as low as 1% of the geophone natural frequency. The presented examples of signals found in the 0.1-1 Hz frequency band emphasize the value of correcting for instrument response both for analyzing recorded signals and for enhancing SNR in virtual shot gathers resulting from interferometric processing.

Within the constraints of a linear array, the most practical way to obtain meaningful subsurface information is to use ambient

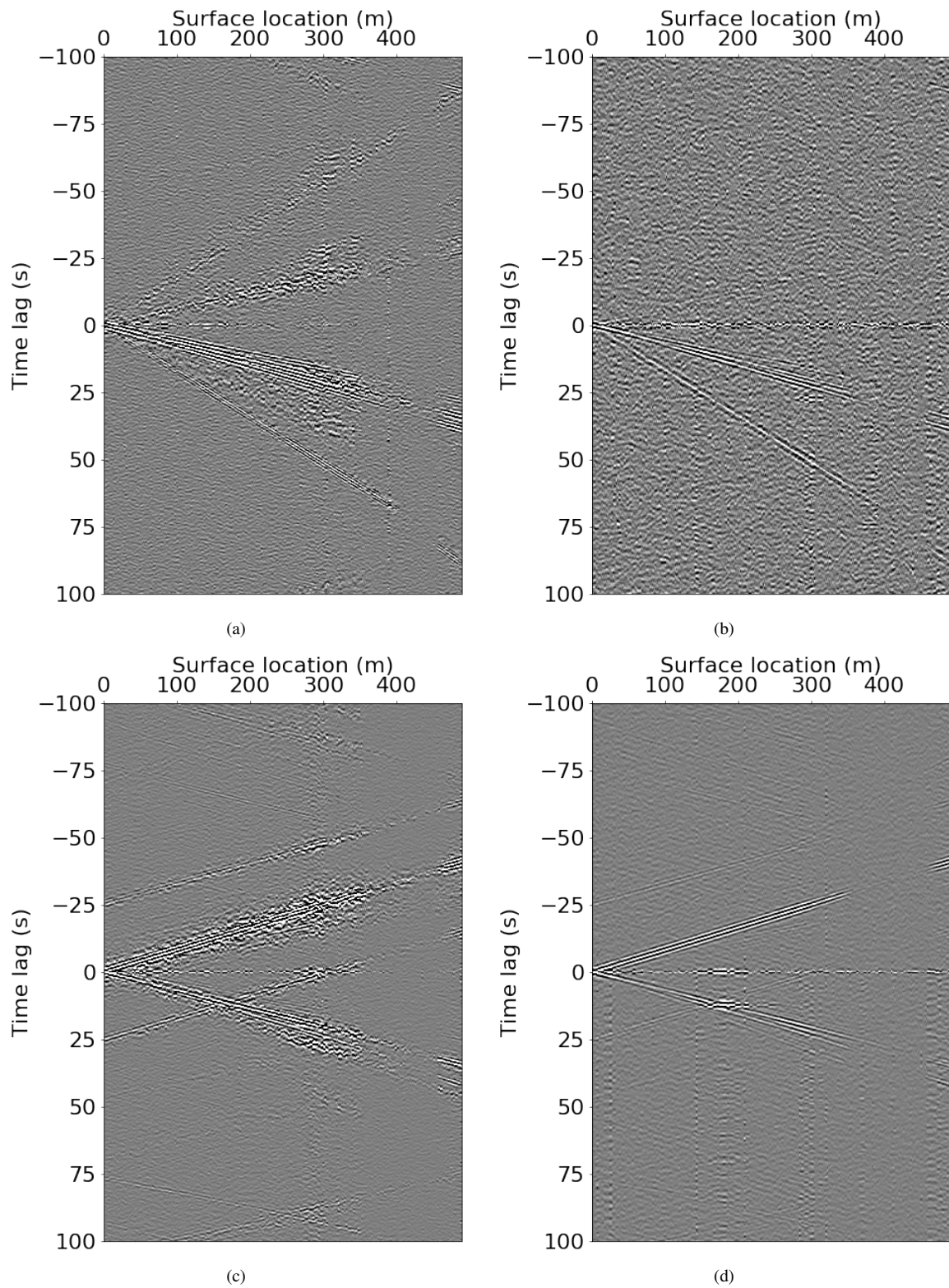


**Figure 9.** Virtual shot gathers created from (a), (b): random noise windows and (c), (d): inline traffic windows in 0.5-1 Hz frequency band. (a) and (c) are formed with raw bandpassed data while (b) and (d) use data after geophone correction and bandpass filter. Correlation panels in this bandwidth are sensitive to the speed of traffic. Correlations after geophone correction show better coherence.

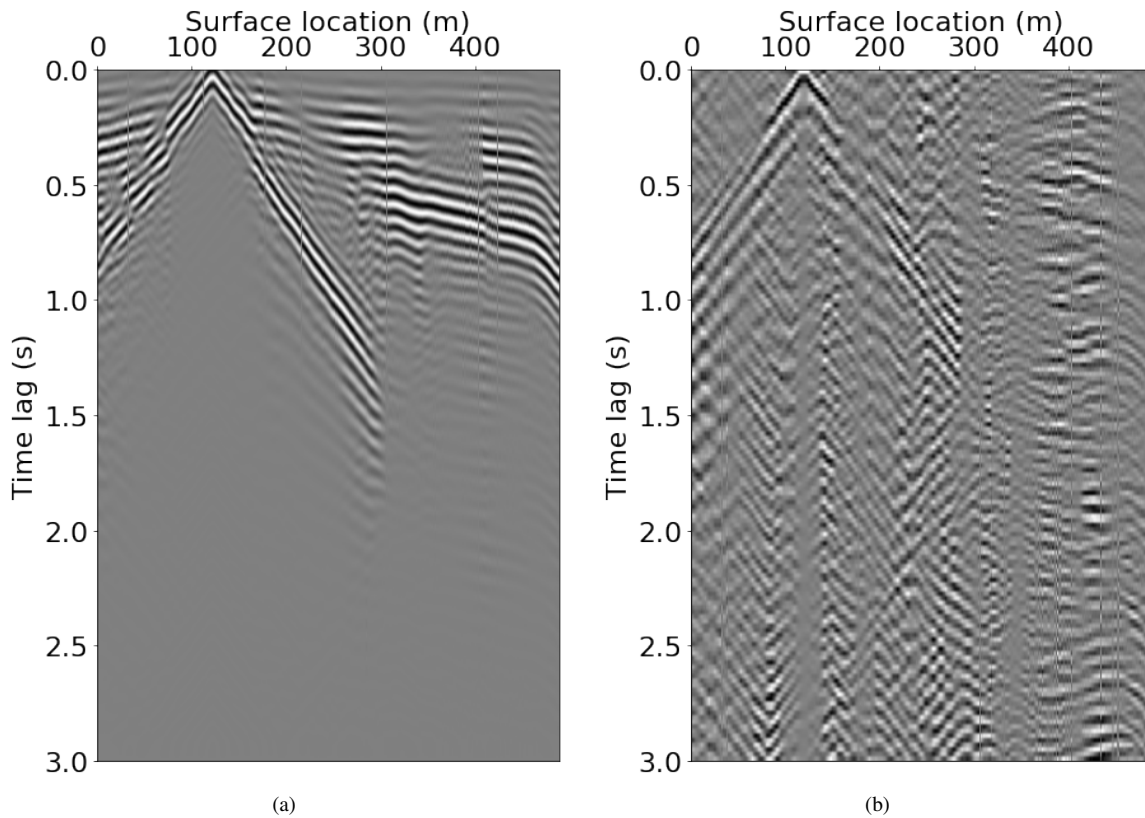


**Figure 10.** Normalized seismic data from (a) an active source shot and (b) virtual gather generated the same surface location as active shot. Active data are bandpassed to match the bandwidth of virtual gather.

data coming from known inline sources such as vehicles moving along the array. At the lowest examined frequencies, the signal associated with local traffic indicates vehicles speed and aside from providing information about local speeding habits, the virtual gathers created from such data may provide information about site attenuation at low frequencies. For a broader bandwidth between 2-20 Hz, moving vehicles also generate surface waves which can be used to derive local shear wave velocity information. We demonstrate that a phase velocity spectrum derived from traffic-generated virtual shot gather compares well with that derived from an active shot in the bandwidth between 5-15 Hz. An added advantage of virtual shot gathers is their ability to fill in the data gaps resulting from skipped shots.

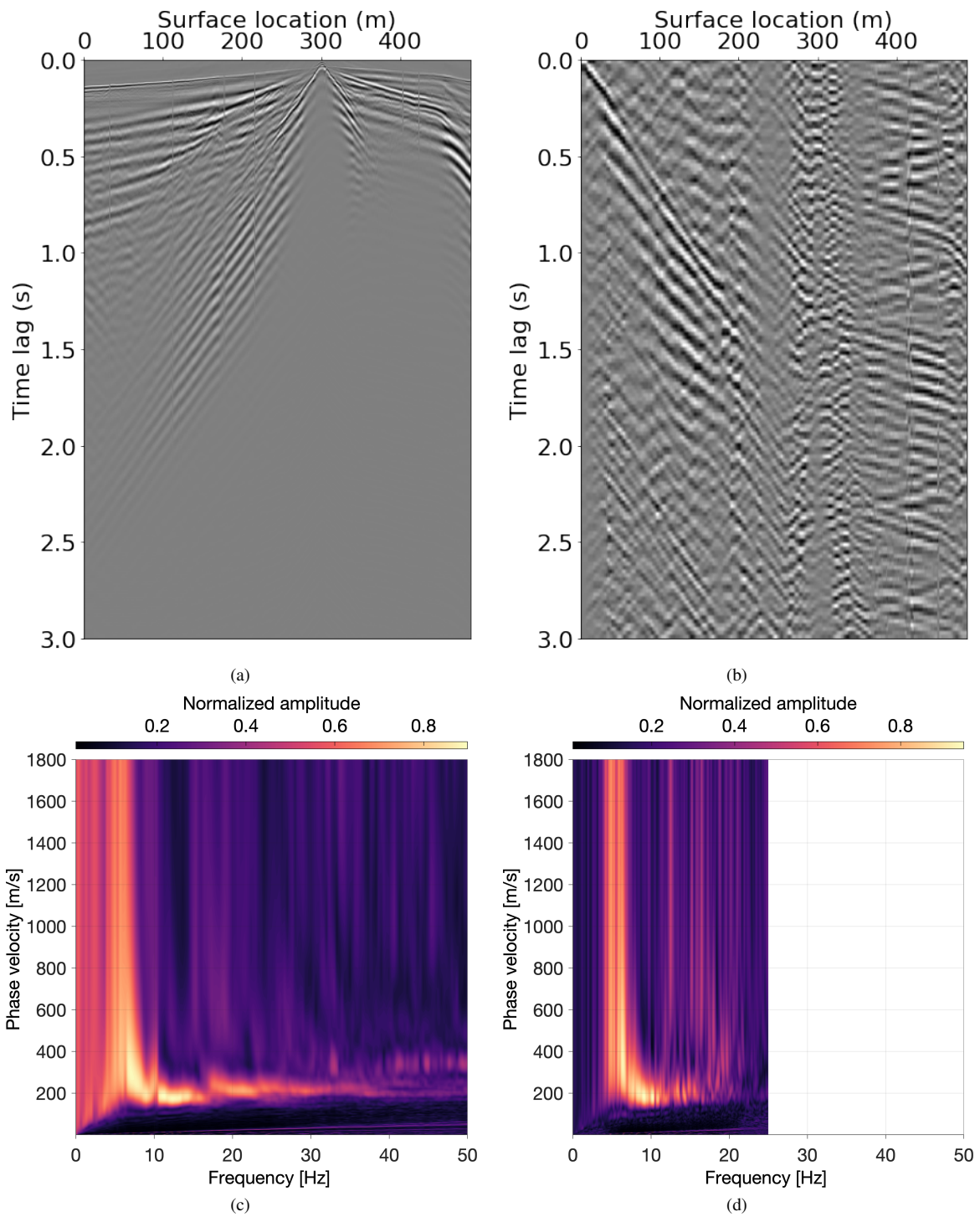


**Figure 11.** Normalized seismic data from (a) an active source shot and (b) virtual gather generated from local traffic data with their respective phase velocity spectra (c),(d). Note that the spectra are similar for 5-15 Hz, with ambient data filling the information gap due to the skipped shots.

## REFERENCES

- Châtenay, A., 2019, Portable seismic survey device and method. (US Patent 10,247,837).
- Dean, T., J. Tulett, and R. Barnwell, 2018, Nodal land seismic acquisition: The next generation: *First Break*, **36**, 47–52.
- Farrell, J., S. M. Wu, K. M. Ward, and F. C. Lin, 2018, Persistent noise signal in the FairfieldNodal three-component 5-Hz geophones: *Seismological Research Letters*, **89**, 1609–1617.
- Freed, D., 2008, Cable-free nodes: The next generation land seismic system: *The Leading Edge*, **27**, 878–881.
- Hons, M., and R. Stewart, 2006, Transfer functions of geophones and accelerometers and their effects on frequency content and wavelets: *CREWES Research Report*, **18**, 1–18.
- Johnson, C. W., F. Vernon, N. Nakata, and Y. Ben-Zion, 2019, Atmospheric processes modulating noise in Fairfield nodal 5 Hz geophones: *Seismological Research Letters*, **90**, 1612–1618.
- Manning, T., C. Brooks, A. Ourabah, M. Popham, D. Ablyazina, V. Zhuzhel, E. Holst, and N. Goujon, 2018, The case for a nimble node, towards a new land seismic receiver system with unlimited channels, *in* *SEG Technical Program Expanded Abstracts 2018: Society of Exploration Geophysicists*, 21–25.
- Mochan, A., 2011, Colorado claims deepest geothermal hot spring record: <https://www.guinnessworldrecords.com/news/2011/9/colorado-claims-deepest-geothermal-hot-spring-record>. (Accessed: 2021-04-10).
- Monk, D. J., 2020, Survey Design and Seismic Acquisition for Land, Marine, and In-between in Light of New Technology and Techniques: *Society of Exploration Geophysicists*.
- Mougenot, D., 2004, Land seismic: Needs and answers: *First Break*, **22**, 59–63.
- Pawelec, I., and P. Sava, 2020, Multiscale analysis and denoising of near offset vibroseis data: *SEG Technical Program Expanded Abstracts 2020, Society of Exploration Geophysicists*, 3264–3268.
- Wang, Y., F. C. Lin, B. Schmandt, and J. Farrell, 2017, Ambient noise tomography across Mount St. Helens using a dense seismic array: *Journal of Geophysical Research: Solid Earth*, **122**, 4492–4508.
- Ward, K. M., and F. C. Lin, 2017, On the viability of using autonomous three-component nodal geophones to calculate teleseismic ps receiver functions with an application to old faithful, Yellowstone: *Seismological Research Letters*, **88**, 1268–1278.
- Wilcox, S., 2015, Equipment QC approaches in land seismic acquisition: *First Break*, **33**, 95–100.